1. Introduction

Liquid crystals (LCs) are well known for its large birefringence that can be easily controlled by external field. According to this, LC-based household appliances have been used widely such as display, TV, etc. Some other LC-based devices like tunable fiber coupler, laser filter and LC-DWDM have been reported by our group. Until recently, optics and applications of LCs have mainly been explored in visible and infrared regime [1, 2]. With the remarkable development of terahertz (THz) technology [3], the research and applications of LCs should be extended to THz range. For this purpose, to measure accurate indices of refraction and the birefringence of LCs is necessary and the first step for THz applications.

In this Chapter, the background information on THz technology, THz time-domain-spectroscopy and nematic liquid crystals are presented. The structure of the thesis is presented in the last part of this chapter as “Thesis highlight”.

1.1. Terahertz technology

Terahertz (THz=10^{12}Hz) radiation represents the last unexplored frontier of the radio wave and light spectrum. The so-called “Terahertz gap” – where until recently bright sources of light and sensitive means of detection have not existed - encompasses frequencies invisible to the naked eyes in the range from 100GHz (10^{11}Hz) up to roughly 30THz ($3x10^{13}$Hz) [3,4]. The former limit lies just above the microwave region where satellite dishes and mobile phones operate, whereas the latter limit is located adjacent to infrared frequencies used in devices such as television remote controllers. The gap is a gray area between microwaves and infrared light

shown in Fig. 1.1.1. Conventional microwave sources do not work fast enough (at high enough frequencies) to efficiently produce radiation in the gap, whereas laser diode sources have been limited by thermal effects. THz quantum cascade laser has just been reported, which has to be operated at very low temperature (~8K). Until recently, scientists were not able to extensively explore the material interactions occurring in the terahertz spectral region—the wavelengths that lie between 30 μm and 1 mm—partly because efficient and reliable sources and detector of terahertz radiation are not available. However, pressure to develop new terahertz sources arose from two dramatically different groups—ultrafast time-domain spectroscopists who wanted to work at longer wavelengths, and radio astronomers who wanted to work at shorter wavelengths. Very recently, advances in ultra-fast pulsed laser technology have led to the generation and detection of broad bandwidth Terahertz light. This dramatic advance was made possible by applying new concepts in semiconductor physics and ultrafast laser systems.

Much of the recent interest in terahertz radiation stems from its ability to penetrate deep into many organic materials without the damage associated with ionizing radiation such as X-rays (albeit without the spatial resolution). Also, because terahertz radiation is readily absorbed by water, it can be used to distinguish between materials with varying water content—for example, fat versus lean meat. These properties lend themselves to applications in process and quality control as well as biomedical imaging. Tests are currently under way to determine whether terahertz tomographic imaging can augment or replace mammography, and some people have proposed terahertz imaging as a method of screening passengers for explosives at

airports. All of these applications are still in the research phase, although TeraView (Cambridge, England) has developed a technique for detecting the presence of cancerous cells that is currently in human trials. THz radiation can also help scientists understand the complex dynamics involved in condensed-matter physics and processes such as molecular recognition and protein folding.

1.2. THz Time-domain-spectroscopy (THz-TDS)

Characterization of LCs and LC devices in the THz frequency range are performed using THz time-domain spectroscopy (TDS) [4]. THz-TDS is a powerful technique that allows broadband THz generation and detection of the field amplitude and phase of the THz wave. A schematic representation of our setup is depicted in Fig. 1.2.1. The light source is a mode-lucked femtosecond Ti:sapphire laser (Spectra Physics Tsunami). The pulses are split into two beams; one constitutes the so-called pump or excitation beam, the other is referred as the probe beam. The pump pulses impinged on a low-temperature grown Gallium Arsenide (LT-GaAs) photoconductive dipole antenna (see Appendix A), acts as a THz emitter. The generated THz pulses are collected and guided by gold-coated parabolic mirrors onto the sample. The incident THz waves on the sample can be also focused by another parabolic gold mirror. The transmitted pulses from the sample are focused by another parabolic gold mirror onto the THz detector, which in our case is also a photoconductive antenna.

This antenna is gated by the optical probe pulse and consists of a metallic dipole antenna, which is constructed on top of a low-temperature grown gallium arsenide (LT-GaAs). The Ti:sapphire laser probe pulse that impinged on the LT-GaAs generates charge carriers and effectively turns the antenna on for a short time interval.

This time interval typically of a few hundreds of femtosecond is determined by the lifetime of the excited carriers. The carriers are accelerated by the THz electric field and then produce a photocurrent. The transmitted THz pulse was monitored by the probe beam from the same laser with a same kind of antenna. The electrical signal of antenna detector is connected to a lock-in amplifier in order to increase the signal/noise ratio. When the optical path length of the two branches of the setup (pump and probe) are equal, the THz and the probe pulse arrive simultaneously to the antenna. By moving a delay stage, the time window in which the carriers are available in the antenna shifts. Hence, by changing this time window it is possible to monitor the time evolution of the THz pulse field.

1.2.1. Antenna-based emitter and detector

While the THz transmitter and receiver designs were identical in early THz TDS works, a wide range of different structures have been investigated, and optimized either for maximum signal or maximum bandwidth. Grischkowsky and coworkers pioneered the coplanar strip line for use as a THz emitter. This structure is appealing for both of the simplicity of the design and the extremely broad emission band [5].

The most commonly used THz receiver design has been a simple dipole antenna, roughly 50μm in length [4]. The collection sensitivity and radiation efficiency of the antenna both vary inversely with the wavelength. Thus, smaller dipole antennas provide a broader bandwidth response; dipoles as small as 30μm have been used. Of course, this 1/λ dependence no longer apply when the radiation wavelength in the substrate becomes comparable to the dipole length, so the details of

the high frequency response are more complex. In addition, the low frequency roll-off in these quasi-optical systems is typically limited by diffraction effects due to the finite size of optical elements such as the substrate lenses. As a consequence, the $1/\lambda$ dependence may apply over only a rather limited spectral range. A detail analysis of THz-TDS system can accurately predict the measured spectral response, as long as all of these effects are taken into account.

If very small dipole antennas are used for both emission and detection, the high frequency limit is mainly determined by the temporal response of the system [6-8]. Another important limitation factor is the response time of the photoconductive material used for substrates of the THz antennas. This limit is more pronounced in the receiver antenna, since one does not expect the highest measured frequency to exceed the inverse of the temporal width of the photo-generated sampling gate, this duration is limited by the carrier trapping time, although a number of schemes have been proposed to avoid this limitation [9,10].

It should be noted that it is possible to detect broadband THz radiation even using a photoconductivity antenna with a slow carrier lifetime. In this case, one relies not on the width of the sampling gate, but merely on its fast-rising edge. If the photocurrent can be modeled as a step function, then the detector operates as a fast sampling gate in an integrating mode, and the measured signal is proportional to the integral of the incident THz field [9]. In this configuration, the bandwidth is limited by the speed of the rising edge of the current, which is determined by the duration of the optical pulse, and by the RC time constant of the antenna [11]. The more detail can be found in Appendix A.

1.2.2. Electro-optical sampling (EOS) in TDS

Historically, freely propagating THz pulses were measured by means of either photoconductive antennas [12-17] or far-infrared interferometric techniques using incoherent detectors such as bolometer [15,16]. Although the photoconductive antennas have excellent sensitivity, their frequency response is limited by resonant behavior of Herzian dipole structure. For the interferometric techniques, the sensitivity is far worse than that the photoconductive antennas, because the measurement is incoherent and its sensitivity is ultimately limited by the thermal background. Besides, the bolometer usually requires liquid-helium cooling. On the other hand, since its first demonstration in 1982 [18], ultrafast electro-optic sampling has been widely used in the measurement of local transient electric field in materials. There existed a need to extend the local field measurement to free space. In 1995, several groups reported their first results using free-space electro-optic sampling independently [19,20]. Later on, it turns out that this technique is a powerful tool for THz pulse measurement, providing many advantages, such as high sensitivity, ultra-broad frequency response, ease of use, and parallel measurement capability [21,22].

There are many different designs of EOS depend on the design of the system and the purpose of the measurement. Here we introduce a typical setup for THz measurement by EOS, which is shown in Fig. 1.2.2.1. The ultrafast laser pulse is split by a beam splitter into two beams: a pump beam and a probe beam. The pump beam illuminates the THz emitter (e.g. a photoconductive-antenna emitter or optical-rectification emitter). The generated radiation is a short electromagnetic pulse with duration on the order of one picosecond, so the frequency is in the THz range. The

radiation normally consists of one cycle or a small number of cycles, so it is broadband. The THz beam is focused by a pair of parabolic mirrors onto an EO crystal. The beam modifies the index ellipsoid of the EO crystal transiently, via the Pockels effect. The linearly polarized probe beam co-propagates inside the crystal with THz beam, and its phase is modulated by the refractive index change induced by the electric field of the THz pulse. This phase change is converted to an intensity change by a polarization analyzer (here a Wollaston prism). Usually a pair of balanced detectors is used to suppress the common laser noise. This also doubles the measured signal. A mechanical delay line is employed to change the time delay between the THz pulse and the probe pulse, and the THz electric field waveform can be obtained by scanning this time delay and performing a repetitive sampling measurement. To increase the sensitivity, the pump beam is modulated by a mechanical chopper, and the THz field induced modulation of the probe beam is extracted by a lock-in amplifier.

1.3. Nematic liquid crystal

The term “liquid crystal (LC)” signifies a state of condensed matter that is intermediate between the crystalline solid and the amorphous liquid. As a rule, a substance in this state is strongly anisotropic in some properties and yet exhibits a certain degree of fluidity, which in some cases may be comparable to that of an ordinary liquid. The first observations of liquid crystalline or meso-morphic behavior were made near the end of 19^{th} century by Reinitzer and Lehmann [24,25]. An essential requirement for the meso-morphism to occur is that the molecules must be highly geometrically anisotropic in shape (rod-like or disc-like). The most common LC phase is the nematic phase. The LCs used in our works is all rod-like nematic LCs.

The nematic ("thread" in Greek) LC has a high degree of long-range orientational order of the molecules. A schematic representation is shown in Fig. 1.3.1. It differs from the isotropic liquid in that the molecules are spontaneously oriented with a common axis, labeled by a unit vector (or "director"). The states of the director $\hat{n}$ and $-\hat{n}$ are indistinguishable in nematic. The director usually varies from point to point in the medium, but a uniformly aligned sample is optically uniaxial with large birefringence. The rotational symmetry of the system can be broken by the particular boundary conditions (ex. Polyimide film, DMOAP coating…etc). The LC molecules around the particularly treated surface tend to orientate with some specific direction, which is the general method to align LCs [26].

If the LC molecules don't orientate parallel to each other, the total energy of the system increases and the deformation exists. Three typical types of the deformation (splay, twist and bend) occur in nematic phase shown in Fig. 1.3.2. The deformation (or distortion) comes from the perturbations of the boundary condition, external field, chiral dopant …etc. The external field, such as electric field or magnetic field, can be used to re-orientate the LC molecules. Briefly, the LC molecules tend to be parallel or perpendicular (mostly parallel) to the field and the extra energy density due to the field is the function of the direction and magnitude of the field. We now consider a strong boundary case, the LC molecules around the boundary will be aligned and some deformation exists in the bulk due to the configuration of the lowest total energy. If we put the external electric/magnetic field on it, the total energy, *F*, can be described as

$$F = \int (f_d + f_{E/M}) d\rho \,. \tag{1.3.1}$$

Where the f_d and $f_{E/M}$ are the extra energy from the deformation and the external electric/magnetic field and ρ is the unit volume. For the parallel case (the LC molecules tend to orientate with the field direction), when the molecules orientate closer to the field direction, the f_d increases and the $f_{E/M}$ decreases. The molecules will be aligned again with the request of the lowest total energy for the stable state. In other words, the deformation term dominates mainly with weak field and the field term dominates for strong field. According to the continuum theory, the director, $\hat{n}$, spatially varies slowly and smoothly and the system keeps the long-range order.

As we have mentioned, the LC molecules tend to be parallel to the director such that the aligned nematic forms an optically uniaxial system. The difference between refractive indices measured with polarization parallel or normal to $\hat{n}$ is quite large. The ordinary index n_o is for light with the polarization perpendicular to the director and the extraordinary refractive index n_e is for light with the polarization parallel to the director. The n_o and n_e of 5CB in visible range are shown in Fig. 1.3.4 [27]. The birefringence, or double refraction of the nematic, is defined as [28]

$$\Delta n = n_e - n_o \,. \tag{1.3.2}$$

When the incident polarization of light is not parallel to the director, the index of the refraction for the extraordinary ray should be written as

$$n_{eff} = \left(\frac{\sin^2\theta}{n_{//}^{\ 2}} + \frac{\cos^2\theta}{n_{\perp}^{\ 2}}\right)^{-1/2}, \tag{1.3.3}$$

where θ is the angle between the propagation direction of the incident light and the optical axis as shown in Fig. 1.3.3. Therefore, the effective birefringence is $\Delta n = n_{eff} - n_o$.

With the undergone remarkable development of the THz techniques, the researchers and the applied scientists have extended the fields into THz gap recently. The optical constants/birefringence of LCs in THz frequency range are the key parameters for either fundamental or applied research.

1.4. Thesis highlights

In Chap. 2, we report the complex optical constants of nematic liquid crystal, 5CB. The temperature of the 5CB sample was controlled with a fluctuation less than 0.1°C. The temperature dependence will also be studied in this chapter. The temperature dependent birefringence of 5CB shows the information about the order parameter of the 5CB, which will be compared with that in visible range.

In Chap. 3, the electrically and magnetically controlled LC THz phase shifters are demonstrated in this chapter. The maximum phase shift of over 2π at 1 THz is achieved by using a sandwich type of LC cell. We also provide several improving method in Sec. 3.4.4.

A tunable THz Lyot filter, which is the further application of the tunable phase shifter will be demonstrated in chapter 4. We use the similar structure of the phase shifter as a tunable retarder. The azimuthal angle of the retarders in the Lyot filter is

not at 45° as usual because of the anisotropic losses of the LC cells. This will be discussed in Sec. 4.5.1. In Chap. 5, we will give a summary about all the works.

Bibliography

1. S. T. Wu, U. Efron, and L. V. Hess, *Appl. Phys. Lett.* **44**, 1033 (1984).
2. I. C. Khoo, R. R. Michael, and G. M. Finn, *Appl. Phys. Lett*. **52**, 2108 (1988).
3. Eric R. Mueller, The Industrial Physicist **27**, Aug./Sept. 2003.
4. Daniel Mittleman, *Sensing with Terahertz Radiation*, 1st ed. (Springer, New York, 2002).
5. S. E. Ralph, D. Grischkowsky, Appl. Phys. Lett. **60**, 1070 (1992).
6. A. Bonvalet, M. Joffre, J.-L. Martin, A. Migus, Appl. Phys. Lett. **67**, 2907 (1995)
7. Q. Wu, X.-C. Zhang, Appl. Phys. Lett. **70**, 1784 (1997).
8. Q. Wu, X.-C. Zhang, Appl. Phys. Lett. **71**, 1285 (1997).
9. F. G. Sun, G. A. Wagoner, X.-C. Zhang, Appl. Phys. Lett. **67**, 1656 (1995)
10. J. Bromage, I.A. Walmsley, C. R. Stroud, Appl. Phys. Lett. **75**, 2181 (1999).
11. S. Kono, M. Tani, G. Ping, K. Sakai, Appl. Phys. Lett. **77**, 4104 (2000)
12. G. Mourou, C. V. Stancampiano, D. Blumenthal, Appl. Phys. Lett. **38**, 470 (1981)
13. D. H. Auston, K. P. Cheung, P. R. Smith, Appl. Phys. Lett. **45**, 284 (1984)

14. A. P. DeFonzo, M. Jarwala, C. R. Lutz, Appl. Phys. Lett. **50**, 1155 (1987)

15. C. Johnson, F. J. Low, A. W. Davidson, Opt. Eng. **19**, 255 (1980)

16. R. C. Johns, J. Opt. Soc. Am. **37**, 879 (1947)

17. C. Fattinger, D. Grischkowsky, Appl. Phys. Lett. **53**, 1480 (1988)

18. J. A. Valdmanis, G. A. Mourou, C. W. Gabel. Appl. Phys. Lett. **41**, 211 (1982)

19. Q. Wu, X.-C. Zhang, Appl. Phys. Lett. **67**, 3523 (1995)

20. P. Uhd Jepsen, C. Winnewisser, M. Schall, V. Schya, S. R. Keiding, H. Helm, Phys. Rev. E **53**, 3052 (1996)

21. Q. Wu, X.-C. Zhang, Opt. Quantum Electron, **28**, 945 (1996)

22. Z. G. Lu, P. Campobell, X.-C. Zhang, Appl. Phys. Lett. **71**, 593 (1997).

23. S. Chandrasekhar, *Liquid Crystals*, 2nd ed. (Cambridge, New York, 1992).

24. F. Reinitzer, Monatsch Chem., **9**, 421 (1888).

25. O. Lehmann, Z. Physikal. Cham., **4**, 462 (1989).

26. P. G. de Gennes and J. Prost, *The Physics of Liquid Crystals*, **2nd ed.** (Oxford, New York, 1983).

27. P. Yeh and C. Gu, *Optics of Liquid Crystal Displays*, **1st ed**. (John Wiley & Sons, New York, 1999).

28. For example, Eugene Hecht, *Optics*, **3rd ed.** (Addison Wesley Longman, New York, 1998).

Figure

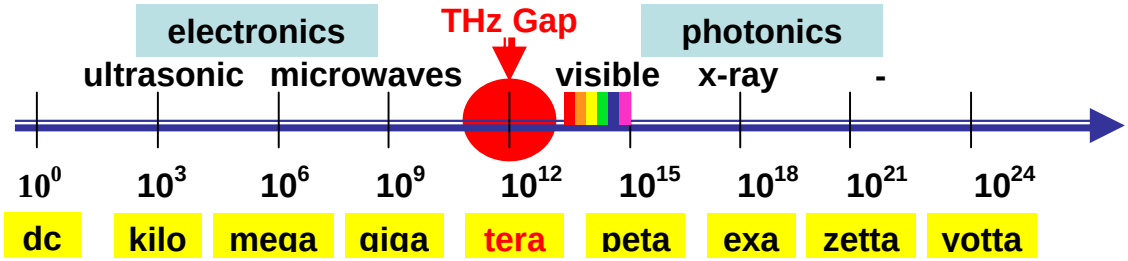

Figure 1.1.1 The diagram shows the name and the applications in different frequency ranges. The THz gap lies between photonics and electronics regimes, which marked as a red area.

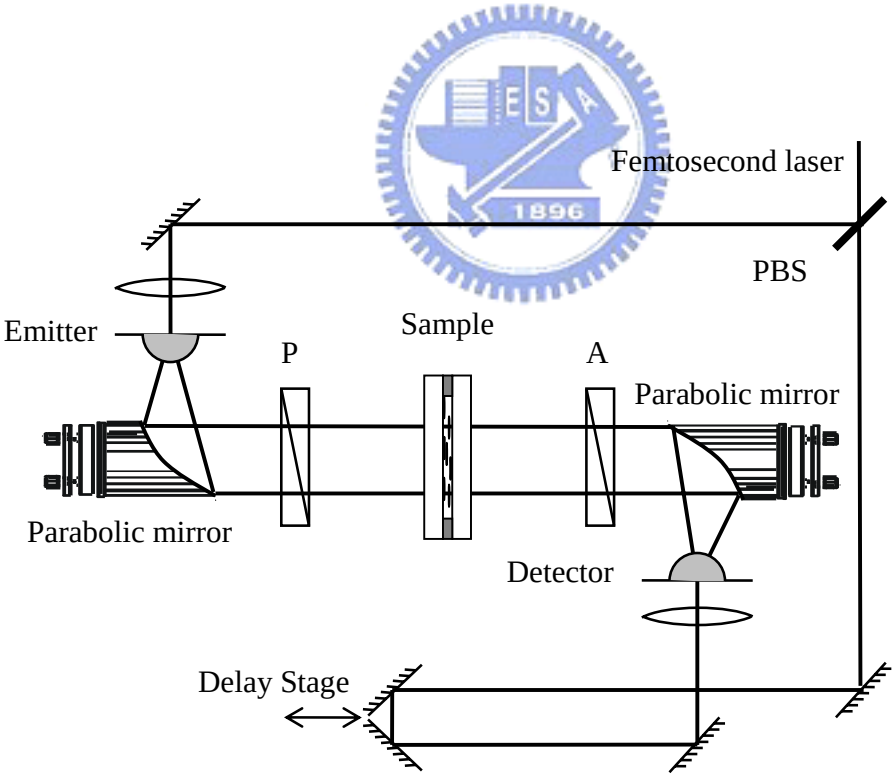

Figure 1.2.1 The general setup of the antenna-based time domain spectroscopy system.

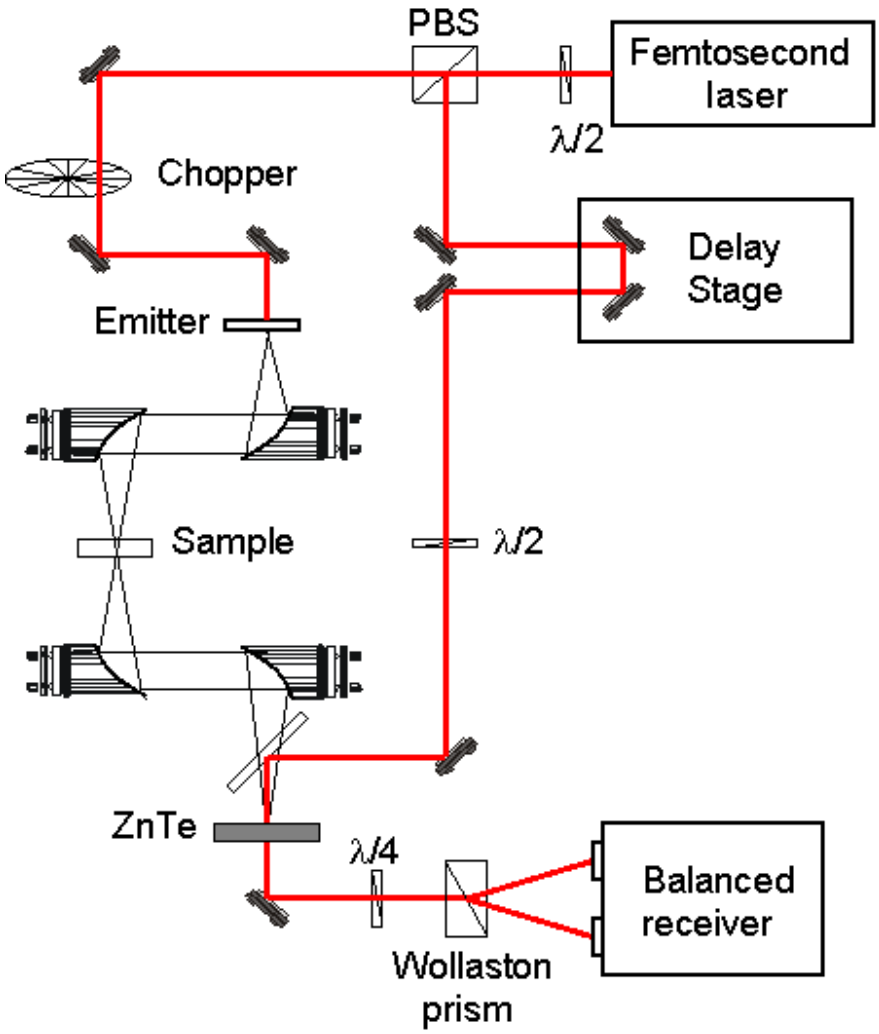

Figure 1.2.2.1 A sample of the electro-optical detection in THz time domain spectroscopy system.

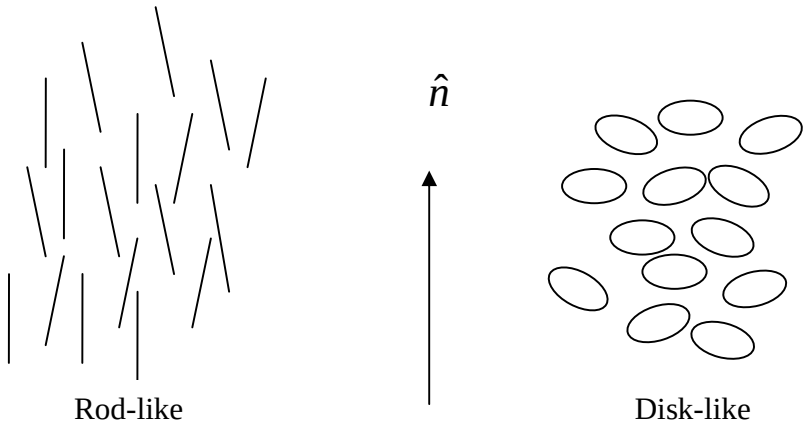

Figure 1.3.1 Schematic representation of molecular order in rod-like and disk-like nematic. The average direction is labeled as director, $\hat{n}$.

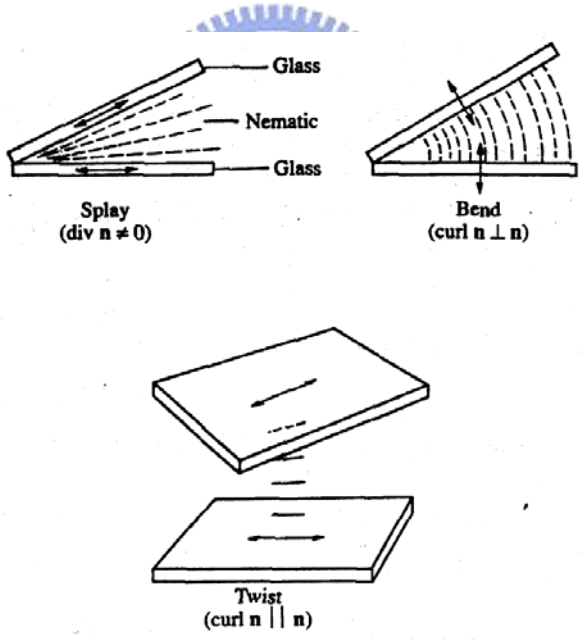

Figure 1.3.2 The three types of the deformation in nematic [26].

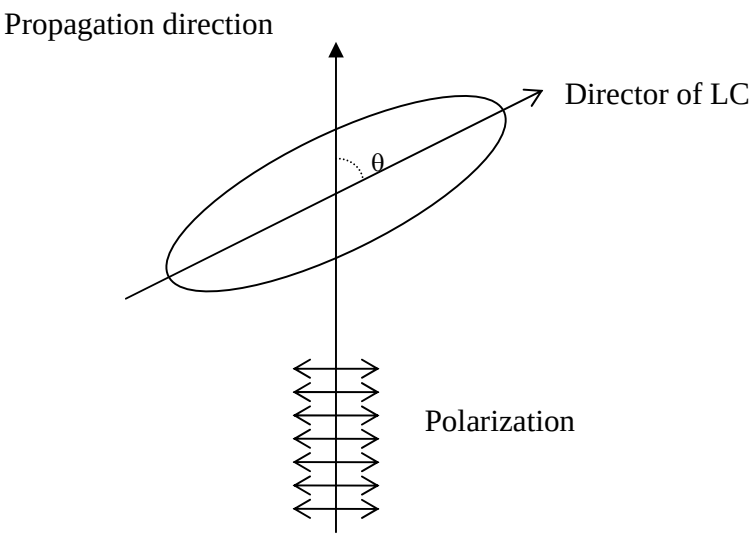

$$n_{eff} = \left(\frac{\sin^2\theta}{n_{//}^{\ 2}} + \frac{\cos^2\theta}{n_{\perp}^{\ 2}}\right)^{-1/2}$$

Figure 1.3.3 The angle, θ, between the long axis and the polarization of the incident electromagnetic wave will affect the effective index of refraction, which the incident light can see.

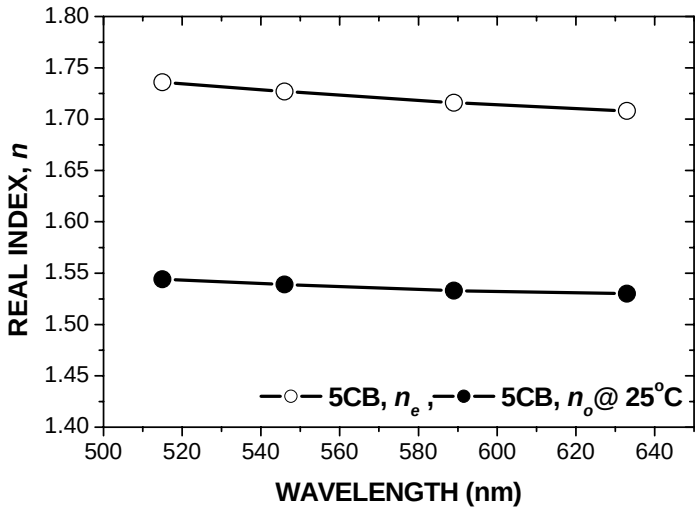

Figure 1.3.4 The refractive indices of 5CB in visible range. The circles and open circles are n_o and n_e respectively [27].